International Journal of Steel Structures (2018) 18:443–455
https://doi.org/10.1007/s13296-018-0016-z

Fatigue Crack Tip Plasticity for Inclined Cracks

Hesham El-Emam[1] · Alaaeldin Elsisi[1] · Hani Salim[1] · Hossam Sallam[2]

Received: 14 February 2017 / Accepted: 26 September 2017 / Published online: 26 April 2018

Abstract

The evaluation of the crack tip deformation is essential to the estimation of crack growth under either static or cyclic loading. A 3-D elastic–plastic finite element analysis was developed to simulate the crack tip deformation along mixed mode inclined edge cracks in a steel plate subjected to either monotonic or cyclic loading at selected R-ratios. In this paper, two types of crack configurations were investigated: inclined cracks with equal inclined lengths (EICL) and inclined cracks with equal horizontal projection length (ECHP). The development of the monotonic (Δm) and cyclic (Δc) crack tip plastically zones and the monotonic (CTOD) and cyclic (ΔCTOD) crack tip opening displacements were traced to find the effect of the crack inclination angle, which significantly affected the size and shape of the crack tip plastic zone. The finite element results compared well with the analytical results based on modified Dugdale's model. It was observed that Mode II has a significant effect on the plastic zone in the case of equal inclined crack length (EICL), i.e., Mode II increases as the crack angle decreases. Also, it is interesting to note that for the EICL case, the magnitude of Δc is delayed to appear with decreasing the inclination angle, for example, for $\theta = 90°$ the cyclic plastic zone appeared at $\Delta\sigma = 103.32$ MPa, while for $\theta = 45°$ the cyclic plastic zone appeared at $\Delta\sigma = 132.84$ MPa. Whereas, the variation of monotonic and cyclic plastic zone size in the equal crack horizontal projection (ECHP) case is not affected by the crack inclination angle. Furthermore, it was observed that the static crack tip opening displacement (CTOD) and the cyclic (ΔCTOD) are independent of the crack inclination angle in case of ECHP, due to such cracks take into consideration the effect of inclination angle through its length.

Keywords Mixed mode I/II · Crack tip displacement · Inclined crack · Plastic zone · Elastic–plastic analysis

List of symbols

w	Plate width
h	Plate height
t	Plate thickness
σ	Applied stress
K_I, K_{II}	Stress intensity factors for modes I and II, respectively
ΔK	Stress intensity factor range
a	Crack length
θ	Angle made by the crack measured in a clockwise direction from the loading axis
R	Stress ratio
CTOD	Monotonic crack tip opening displacement normal to the crack face
CTSD	Monotonic crack tip sliding displacement
$CTOD_R$	Resultant of monotonic normal and sliding opening displacements
$\Delta CTOD_R$	Resultant of cyclic normal and sliding opening displacements
Y	Geometry correction factor
Δm	Monotonic plastic zone size (MPZS)
Δc	Cyclic plastic zone size (CPZS)
FCG	Fatigue crack growth
ε_y	Engineering tensile yield strain
σ_y	Engineering tensile yield strength
μ	Poisson's ratio
E	Young's modulus
ECHP	Equal crack horizontal projection
EICL	Equal inclined crack length

Hesham El-Emam and Hossam Sallam—On leave from Materials Engineering Department, Zagazig University, Zagazig, Egypt.

✉ Hesham El-Emam
elemamh@mail.missouri.edu

[1] Civil and Environmental Engineering, University of Missouri, Columbia, MO 65211, USA

[2] Civil Engineering, Jazan University, Jazan, Kingdom of Saudi Arabia

1 Introduction

The estimation of the crack tip plastic deformation is important to the evaluation of crack growth under either static or cyclic loading. Different approaches have been proposed in the past to connect the fatigue crack growth with applied driving forces. Earliest effort correlated the applied stress level with failure time (Zhang and Liu 2011). Cracks under mixed mode loading can be found in various engineering structures. The remaining life of such cracks subjected to cyclic loading depends largely on the rate and direction of the growth behavior of the crack, which should be better understood. The initial crack direction and its subsequent growth and path prediction is a classic fatigue problem. Considerable research efforts have been focused on experimentally investigating fatigue crack growth (FCG) behavior under mixed mode I/II loading (Hammouda et al. 2003a, b; Qian and Fatemi 1996, 1999; Wong et al. 2000; You and Lee 1998; Plank and Kuhn 1999; Reddy and Fatemi 1992).

CTOD (δ) approach was first developed by Wells (1963). A significant amount of plasticity occurs at the crack tip, and the fracture process is controlled by maintaining a critical strain adjacent to the crack tip, which can be measured by the CTOD (Hannachi and Djebaili 2013). Dugdale (1963) suggested a "strip yield" model for perfectly plastic non-strain hardening metals that provides a plastic zone size in plane stress. CTOD derivation was illustrated using an edge crack in a finite width plate under pure mode I. The CTOD under monotonic loading can be expressed as Dugdale (1963), Tada et al. (1973) and Suresh (1998):

$$CTOD = \frac{K_I^2}{E\sigma_y} = \lambda\sigma^2 a \tag{1}$$

where $\lambda = \frac{Y^2\pi}{E\sigma_y}$, E is the Young's modulus, and σ_y is the yield strength. K_I *is* the mode I intensity factor (SIF), which σ is to be corrected by multiplying with a geometric correction factor Y as Isida (1966):

$$\begin{aligned} Y(a/w) =& 1.12 - 0.231(a/w) + 10.55(a/w)^2 \\ & - 21.22(a/w)^3 + 30.39(a/w)^4 \end{aligned} \tag{2}$$

where a *is* the crack length and w is the plate width.

An estimation of the monotonic plastic zone size, Δm ahead of the crack tip in ductile solids has been derived to quantify the near tip fields for the linear elastic crack in terms of stress intensity factor. The extent of the plasticity affected zones is Dugdale (1963), Tada et al. (1973) and Suresh (1998):

$$\Delta m = \frac{\pi}{8}\left(\frac{K}{\sigma_y}\right)^2 \tag{3}$$

Chang and Guo (1999) stated that the reversed plastic zone (Δc) acted as a dominant factor for the behavior of the fatigue cracks. Some researchers (Para et al. 1996) suggested that the reversed plastic zone size would be a better parameter for fatigue crack growth if the effects of the applied stress level, specimen thickness and crack closure are taken into account. Rice (1967) reviewed the mathematical models for the analysis of fatigue crack growth. He concluded that for a plane stress case, the cyclic plastic zone size (Δc) is defined by:

$$\Delta c = \frac{1}{4}\Delta m \, at \, R = 0 \tag{4}$$

As is already known, the crack tip suffer from compressive stresses greater than the yield strength of the material at the end of the unloading cycle even, in positive applied stress ratio. Therefore, the yield stress during unloading ranges from $+\sigma_y$ to $-\sigma_y$ or $2\sigma_y$ which is twice the value for monotonic loading. Based on this, (McEvily 2009) concluded that the cyclic crack-tip opening displacement (ΔCTOD) was one-half of that obtained under monotonic loading, i.e.,

$$\Delta CTOD = \frac{(\Delta K)^2}{2\sigma_y E} \tag{5}$$

where, ΔK is the stress intensity factor range ($K_{max} - K_{min}$).

However, this conclusion is not accurate since crack closure behavior was not accounted for this formulation. When (Elber 1970, 1971) discovered crack closure, he proposed that for cyclic loading, the significant parameter in crack growth is ΔK_{eff}, where $\Delta K_{eff} = K_{max} - K_{op}$; K_{op} being the value of the stress intensity factor at the crack opening level. Equations (1)–(5) specify the CTOD and plastic zone size variation during a single cycle. If the applied loading is maintain data constant amplitude, Eqs. (1)–(5) can be used to predict the variation of the plastic zone and the crack tip opening displacement. El-Emam et al. predicted the delay of fatigue crack growth in the structural steel elements due to bonded composite patch by either LEFM (El-Emam et al. 2017) or EPFM (El-Emam et al. 2016) and they approved that crack tip deformation parameter (CTDP) proposed by Hammouda et al. (1995, 1999, Hammouda et al. 2004a, b) is a logical candidate for such a task, which takes into account the effect of fatigue crack closure on the development of crack tip plastic zones and crack tip opening displacements under pure mode I. Therefore in this paper, a 3D finite element analysis was developed to simulate the crack tip deformation parameters along mixed mode I/II inclined edge cracks in a steel plate subjected to either monotonic or cyclic loading at R-ratio equals zero. The finite element results compared with the analytical results based on modified Dugdale's model. Two types of crack configurations were investigated: inclined cracks with equal inclined lengths (EICL) and inclined cracks with equal horizontal projection length (ECHP). The development of Δm, Δc, CTOD, and ΔCTOD were traced at different mode-mixity, i.e., different crack inclination angles.

2 Finite Element Analysis

The numerical simulation was performed using ANSYS 14.5. Bilinear kinematic hardening plastic simulation is performed in order to calculate the crack tip deformation parameters, i.e., Δm, Δc, CTOD and ΔCTOD. Most of existing elasto-plastic models have used the isotropic hardening rule. But, the main cyclic plasticity response, like Bauschinger effect, cannot be included by the isotropic hardening rules (Paul and Tarafder 2013). Therefore, the kinematic hardening model to obtain the cyclic response at the crack tip during the cyclic loading was used in the present work. Advance cyclic plasticity model (kinematic hardening model) was adopted for the analysis.

The back stress tensor for bilinear kinematic hardening evolves so that the effective stress versus effective strain curve is bilinear. The initial slope of the curve is the elastic modulus of the material and beyond the user specified initial yield stress σ_y, plastic strain develops and the back stress evolves so that stress versus total strain continues along a line with a slope defined by the user specified tangent modulus ET. This tangent modulus cannot be less than zero or greater than the elastic modulus. For uniaxial tension followed by uniaxial compression, the magnitude of the compressive yield stress decreases as the yield stress increases so that the magnitude of the elastic range is always $2\sigma_y$, as shown in Fig. 1.

2.1 Geometrical Model and Loading

Figure 2 shows an inclined edge crack in a steel plate, with a varying crack angle θ (90°, 60°, and 45°). The plate used in the FE model represented in the global coordinates (x, y) and has the following dimensions: 300 mm × 150 mm with a thickness of 6 mm. The length of the crack is a (30, 45, and 60 mm), and the crack is assumed to occur in the r-direction (r-θ coordinate system), i.e., mixed mode I and II cracks are considered. The plate was tested under a uniaxial tensile fatigue load of $\sigma_{max} = 150$ MPa. The fatigue loading for this study was set at the stress ratio of zero. The stress ratio is the ratio of the minimum stress to the maximum stress of the specimen during the fatigue test:

$$\sigma_{min} / \sigma_{max} = 0.0$$

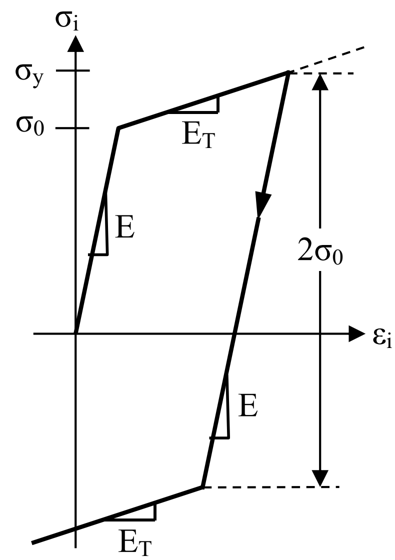

Fig. 1 Illustration of the bilinear kinetic hardening model

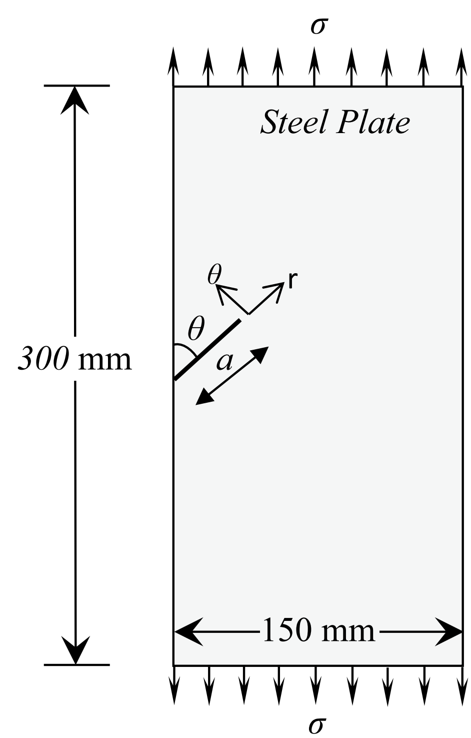

Fig. 2 Geometrical model of cracked plate

The maximum force applied in the fatigue load block was 135 kN. The 0–135 kN range applied a stress range of 150 MPa on the specimens.

2.2 FE Modeling

A fracture analysis is a combination of stress analysis and fracture mechanics parameters calculation. The stress analysis is a standard linear elastic or nonlinear elastic plastic analysis. Because high stress gradients exist in the region around the crack tip, the FE modeling of a component containing a crack requires special attention in that region (ANSYS Decumentation). For linear elastic fracture mechanics (LEFM) problems, the displacements near the crack tip (or crack front) vary as $\sqrt{r}$, where r is the distance from the crack tip. The stresses and strains are singular at the crack tip, varying as $1/\sqrt{r}$. LEFM can predict the monotonic and cyclic crack tip plastic deformation in the case of small scale yielding. Therefore, the singular element used in the elastic analysis is adopted in the present work. To resolve the singularity in strain, the crack faces should be coincident, and the elements ahead of the crack tip should be quadratic, with the mid-side nodes placed at the quarter points; such elements are called singular elements. ANSYS provides an option which permits extruding any 2D mesh with 2D elements to 3D mesh with 3D solid elements. This technique is suitable for the modeling of 3D through-thickness cracks, which requires solid elements with mid-side nodes, such as SOLID186. Accordingly, the calculation of the Fracture Parameters along the crack front can be readily obtained. Figure 3 shows the 3D singular element and division around the crack tip.

Figure 4 shows the mesh and boundary conditions used to model single edge cracked plate. The steel plates were simulated by 20 nodes SOLID186 elements, having three degrees of freedom per node (translations in the nodal x, y, and z directions) as shown in Fig. 4a. Figure 4b details the crack-tip mesh formulation surrounding the crack of the edge cracked steel plate. Per the meshing guidelines of ANSYS, mesh refinement was implemented in the vicinity of the crack tip: 60 elements (6° per element) were used around the circumferential direction so that a sharp crack tip was created to generate singularity. The ratio between the first and second rows of these elements was set to be 0.75. The crack length used is a = 45 mm with different inclination angles, θ = 90, 75, 60, and 45 degrees. The material used is steel with a Young's modulus E of 200 GPa, a Poisson's ratio ν of 0.3, a yield strength σ_y of 360 MPa, and a tangent modulus E_T of 2 GPa. A sensitivity analysis was performed to evaluate the effect of mesh density ahead of the crack tip on stress intensity factors as shown in Fig. 5. The size of singular elements around the crack tip was varied from 1 to 10% of the crack length. It was found that convergence was achieved when the element size around the crack tip was at 8% or below, which is consistent with ANSYS recommendations.

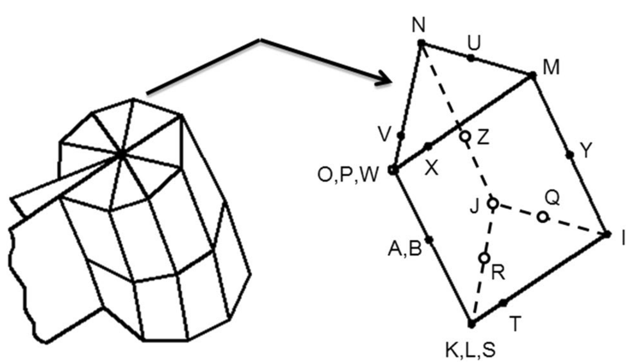

Fig. 3 3D singular element and division around the crack tip

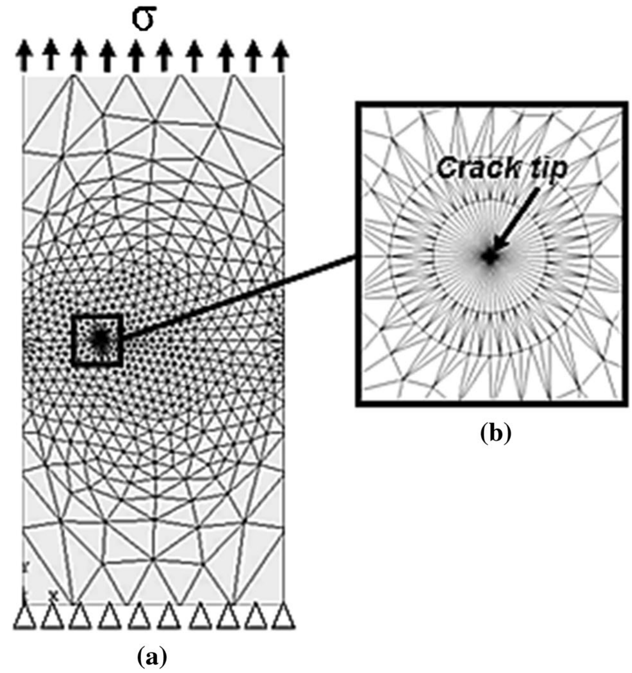

Fig. 4 Illustration of the FE model: **a** FE grid for the finite width plate with an edge crack; **b** detailed view of mesh refinement in the vicinity of the crack tip

3 Validation

To validate the present finite element analysis (FEA), a comparison between the FE results of this paper and the well-known analytical equations were made as follows:

3.1 K_I and K_{II} Measured for Different Crack Angles

A plate with a width (w) of 150 mm, a height (h) of 300 mm, and a thickness (t) of 6 mm having a single edge through-thickness crack was used for verification with analytical models. Two crack length: a = 30 and 45 mm, such that

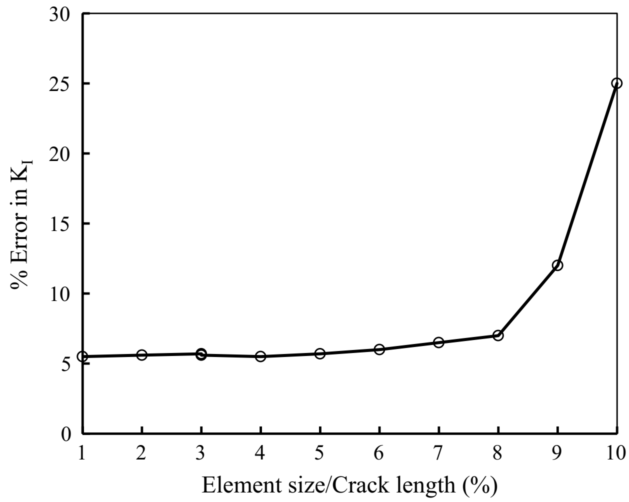

Fig. 5 Convergence study of % error in K_I of a plate with edge crack under tensile load

a/w = 0.2 and 0.3 were used in this section. The cracks were analyzed for different angles: θ = 90, 75, 60, and 45 degree. The plates were subjected to either monotonic or cyclic loading at a stress ratio R = 0. Tetrahedral elements with 20 nodes describing each element were used in the FE modeling with an element size of 0.05 mm in the fine region around the crack tip. The element size was small enough to accurately capture both the monotonic and cyclic plastic deformation existing around the crack front. The crack front was located in the fine mesh region.

Figure 6 shows the SIF (K_I and K_{II}) values for the different values of the crack inclination angle θ. The analytical values obtained from Stress intensity factor handbook (Murakami 1987) were compared to the FE values for both K_I and K_{II}, which show good agreement as shown in Fig. 6. A difference of a maximum of 8% is observed compared to the analytical solution.

3.2 CTOD and Δm at θ = 90 Degrees for Different Crack Lengths Under Constant K

The CTOD predicted by the FE was defined as the displacement at the intersection of a 90-degree vertex with the crack faces, which is behind the crack tip, as shown in Fig. 7. An automated ANSYS Parametric Design Language (APDL) code is used to determine the CTOD at every load step in ANSYS to track the CTOD variation under cyclic loadings. The stress intensity factor K was held as a constant for the different crack lengths to obtain a reasonable monotonic and cyclic plastic zone size. The plastic zone size (Δm) represented in this work as the diameter of the circle which has the same area of the plastic zone around the crack tip. The applied stress with stress ratio of zero for the different crack lengths, a/w = 0.2, 0.3, and 0.4, are shown in Table 1.

The normalized monotonic CTOD and MPZS (Δm) variations for every applied stress step are shown in Fig. 8. The FE results of this paper are compared to the analytical calculations from Eqs. (1 and 3) that are based on the modified Dugdale's models (Dugdale 1963; Tada et al. 1973; Suresh 1998). Figure 8 shows that the analytical approximation is in agreement with the FE solutions. A maximum difference of 8% can be observed compared to the analytical solution.

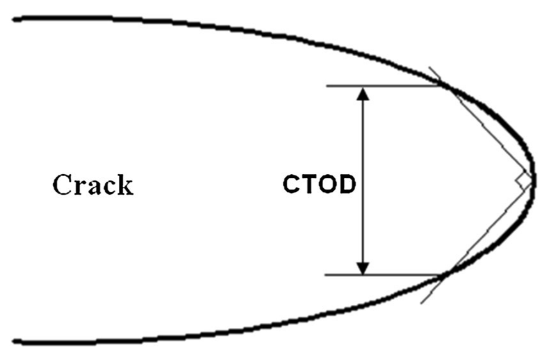

Fig. 7 Schematic of CTOD behind the crack tip

Fig. 6 Comparison between the FE and analytical results for SIF KI and KII for different inclined edge crack angles

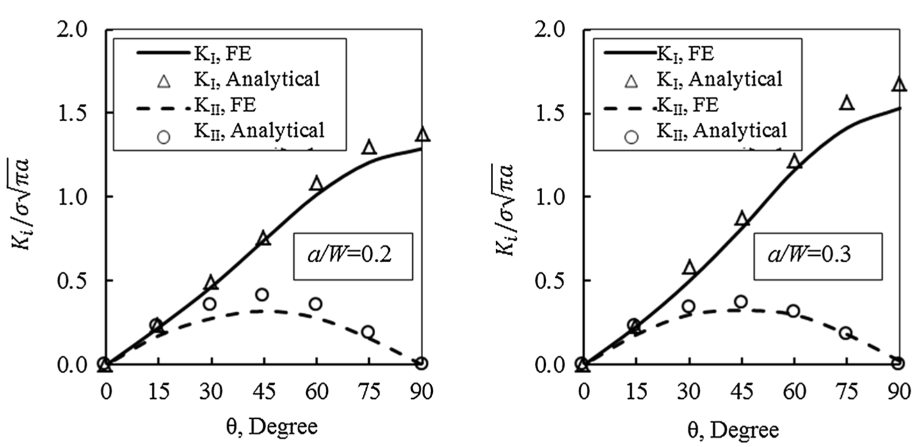

Table 1 Loading with constant stress intensity factor K_I for different crack lengths

a/w	Uniaxial stress (σ) MPa	Geometric correction factor (Y)	Stress intensity factor, K_I
0.2	220.4	1.37	92.7
0.3	147.6	1.67	92.7
0.4	100.0	2.13	92.7

3.3 ΔCTOD and Cyclic Plastic Zone Size Under Constant K

The calculation of ΔCTOD in ANSYS during the unloading part was the same as the loading part. The cyclic plastic zone size (Δc) calculated as the diameter of the circle which has the same area of the plastic zone around the crack tip during the unloading part. An APDL code is used to calculate the ΔCTOD at every loading step in ANSYS to trace its variation. Figure 9 shows the normalized cyclic ΔCTOD and CPZS (Δc) variations as a function of the applied stress. As shown in the Fig. 9, the FE solutions are in agreement with analytical calculations from Eqs. (4 and 5) with a maximum difference of 20%.

4 Analysis of Results

The results of the FEA are evaluated for two types inclined crack descriptions in terms of the monotonic and cyclic plastic zone sizes. Two different inclined crack descriptions were numerically analyzed with the different crack inclination angle θ as shown in Fig. 10. The first category is equal crack horizontal projection (ECHP), where the length (a) is the horizontal projection of the inclined crack length. The second category is described by equal inclined crack lengths (EICL), where the length (a) is the length along the crack in the polar (inclined) direction.

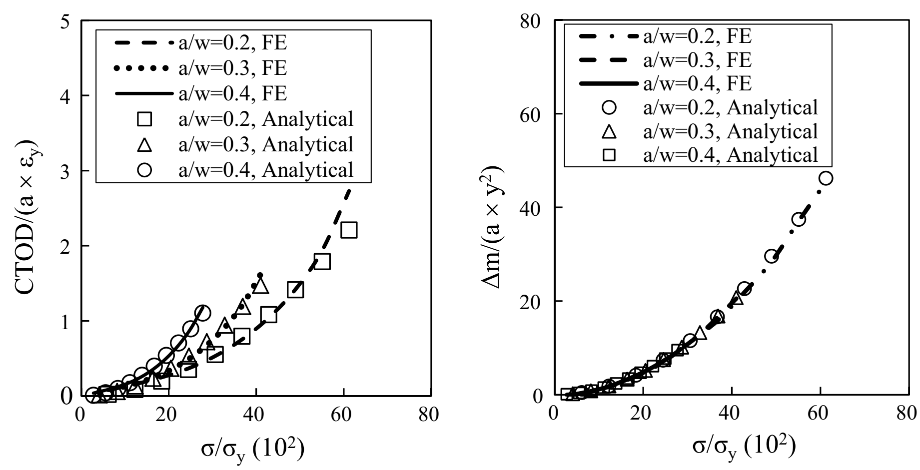

Fig. 8 Comparison between the FEM result and the proposed theoretical result for CTOD and Δm versus the applied stress σ

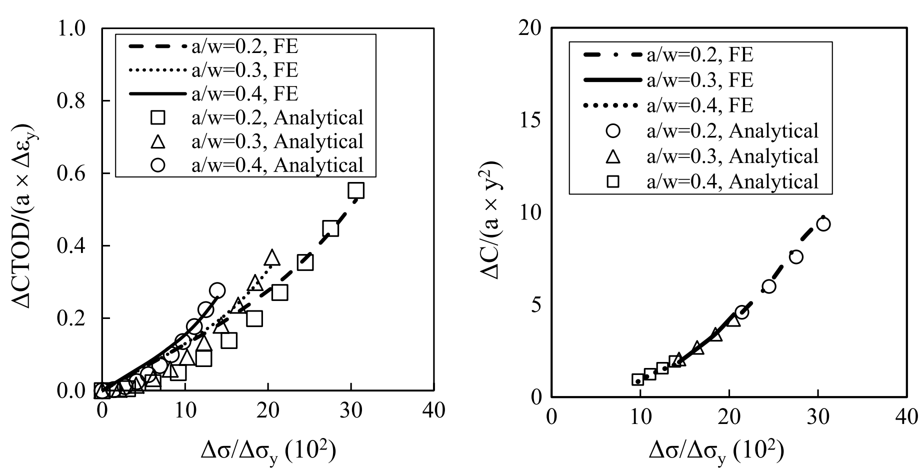

Fig. 9 Comparison between the FEM result and the proposed theoretical result for ΔCTOD and ΔC versus the applied stress σ

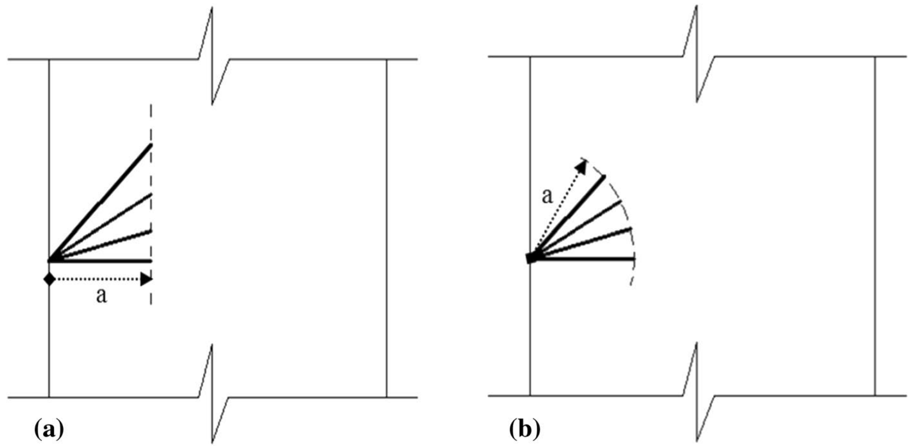

Fig. 10 Inclined crack descriptions: **a** cracks with equal horizontal projection length (ECHP); **b** equal inclined crack lengths (EICL)

4.1 Monotonic and Cyclic Plastic Zones Development

Figures 11 and 12 present the development of both monotonic and cyclic PZS for the two categories EICL and ECHP against the applied stresses during the first load cycle for the analyzed stress ratios R = 0. It was found that, in the case of ECHP, the monotonic plastic zone size, Δm is increase during the loading process. Furthermore, at any applied stress the size of the plastic zone is the same for the different crack angles. In the un-loading part when the load approached a zero value, the pair of nodes at the crack mouth was closed first followed by a sequence of crack surface closures towards the tip as shown in Fig. 13. That was a normal crack closure process usually found in the case of a stationary crack (Hammouda et al. 1995) due to the absence of compressive residual stresses behind the crack tip. Also due the Bauschinger's effect, the cyclic plastic zone can be detected at the last steps of the unloading part. It is also evident that the areas of the cyclic plastic zone in the case of ECHP are almost equal at the same load with the different crack angles. In the case of EICL, the monotonic plastic zone increases during the loading part, but when the crack inclination angle decreases the plastic zone decreases

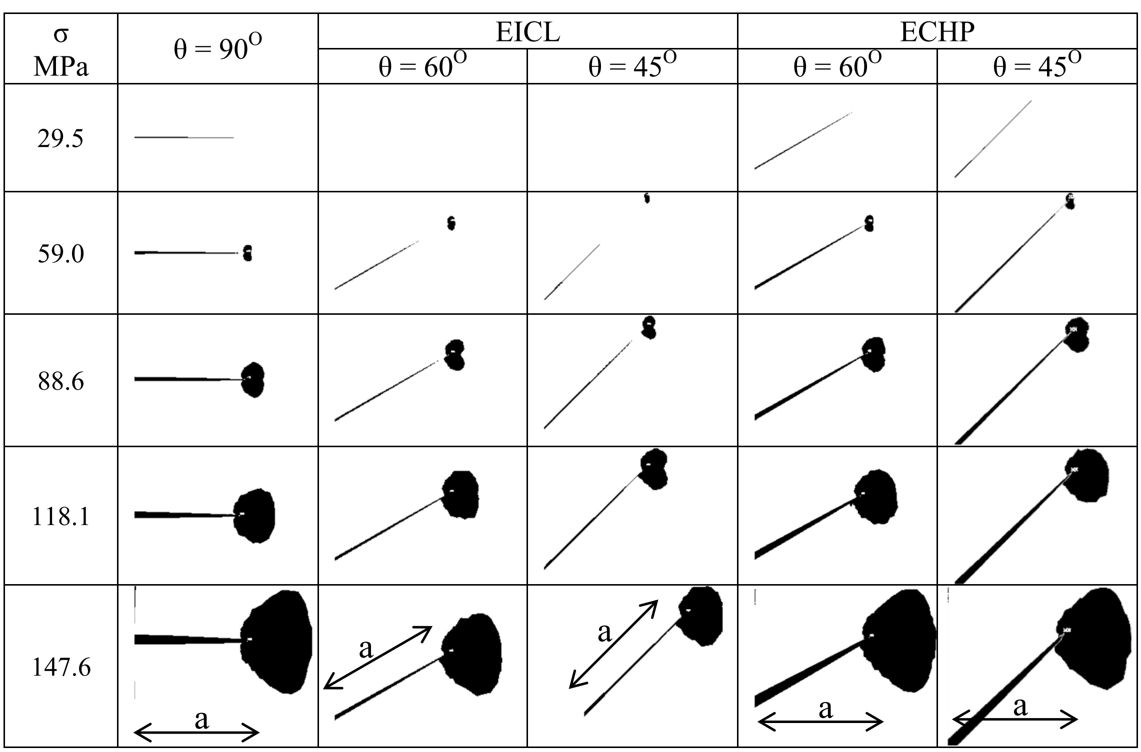

Fig. 11 Monotonic plastic zones developed ahead of the crack tip for ECHP and EICL cases

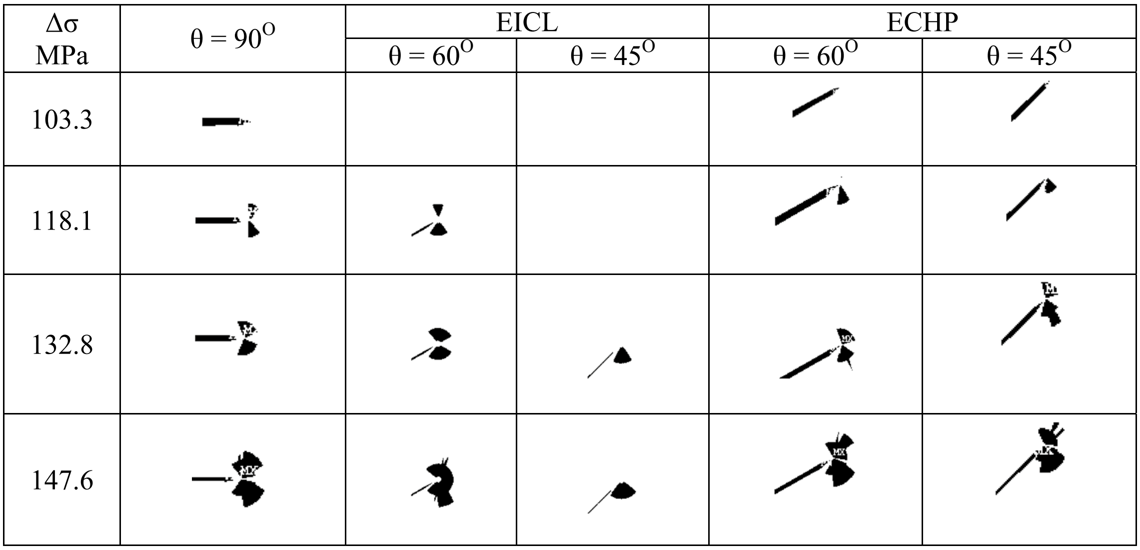

Fig. 12 Cyclic plastic zones developed ahead of the crack tip for ECHP and EICL cases

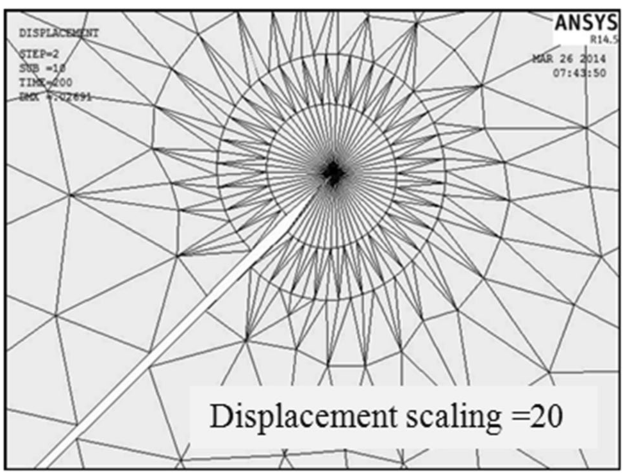

Fig. 13 Sequence of crack surface closure towards the tip

as shown in Fig. 11. Moreover, it is interesting to note that for the EICL, the magnitude of Δc is delayed to appear with decreasing the inclination angle θ, i.e., for θ = 90 degrees the cyclic plastic zone appeared at Δσ = 103.32 MPa, while for θ = 60 degrees it appeared at Δσ = 118.1 MPa, and for θ = 45 degrees it appeared at Δσ = 132.84 MPa.

4.2 Plastic Zones for Different Crack Angles

The shape and size of the plastic zone is shown in Fig. 14 for the two different crack categories at various crack inclination angles, θ = 45, 60, 75, and 90 degrees. Figure 14b shows that the size of the plastic zone increases with the increment of the crack inclination angle θ for EICL. The plastic zone had two non-symmetrical lobes except for the case of θ = 90°. Similar results were obtained by Soh and Bain (2001) and Hammouda et al. (2002), (2003a, b). Figure 14a shows the size of the plastic zone in the case of ECHP. It was observed that, the size of the plastic zone remained the same with the increase of the crack inclination angle θ, and the plastic zone approximately had two symmetrical lobes. This observation indicates that Mode II has a significant effect on the plastic zone in the case of EICL, i.e., Mode II increases with the decrease of angle θ, while it has very little effect on the plastic zone in the case of ECHP.

4.3 Δm and Δc for ECHP

The variation of normalized monotonic plastic zone size (Δm/a) versus the normalized applied stress (σ/σ_y) for a/w = 0.3 is shown in Fig. 15a. It is interesting to note that the variation of Δm/a versus σ/σ_y has a polynomial trend and the normalized monotonic plastic zone size are the same for different crack inclination angles in case of ECHP. The proportionality constant can be evaluated by fitting a polynomial equation to the Δm data. From these results, the relation between (Δm/a) and (σ/σ_y) independent of the crack inclination angle can be expressed as:

$$\Delta m = a\left[4.79\left(\frac{\sigma_i}{\sigma_y}\right)^2 - 0.35\left(\frac{\sigma_i}{\sigma_y}\right) + 0.017\right] \quad \text{for } a/w = 0.3 \tag{6}$$

For the normalized cyclic plastic zone size (Δc/a), Fig. 15a shows that the variation of Δc/a versus σ/σy has a linear trend and the normalized cyclic plastic zone size has a little different quantities for different crack inclination

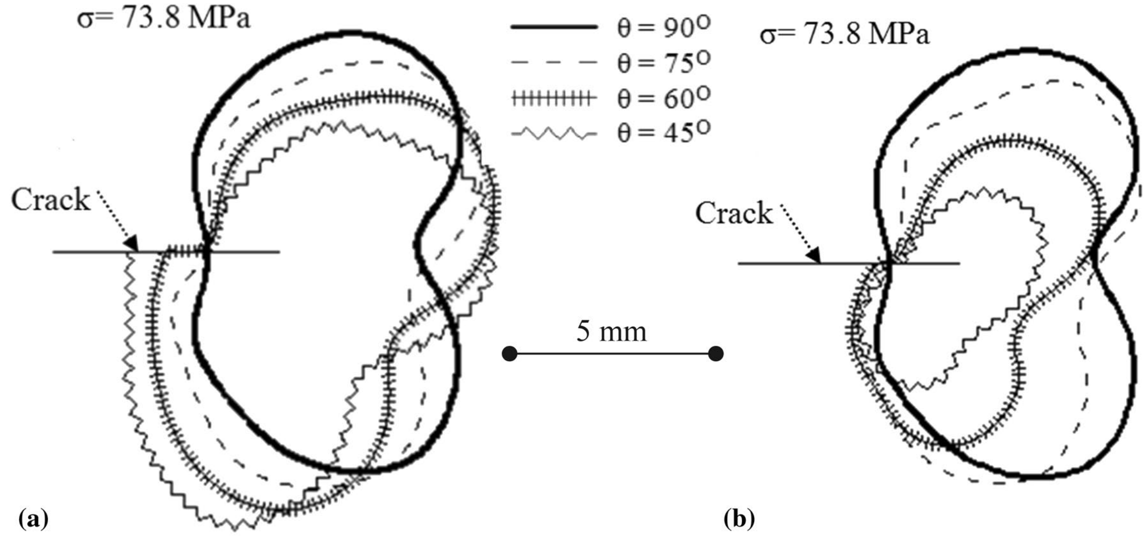

Fig. 14 Von Mises crack-tip plastic zone for different inclination angles θ: **a** ECHP; **b** EICL

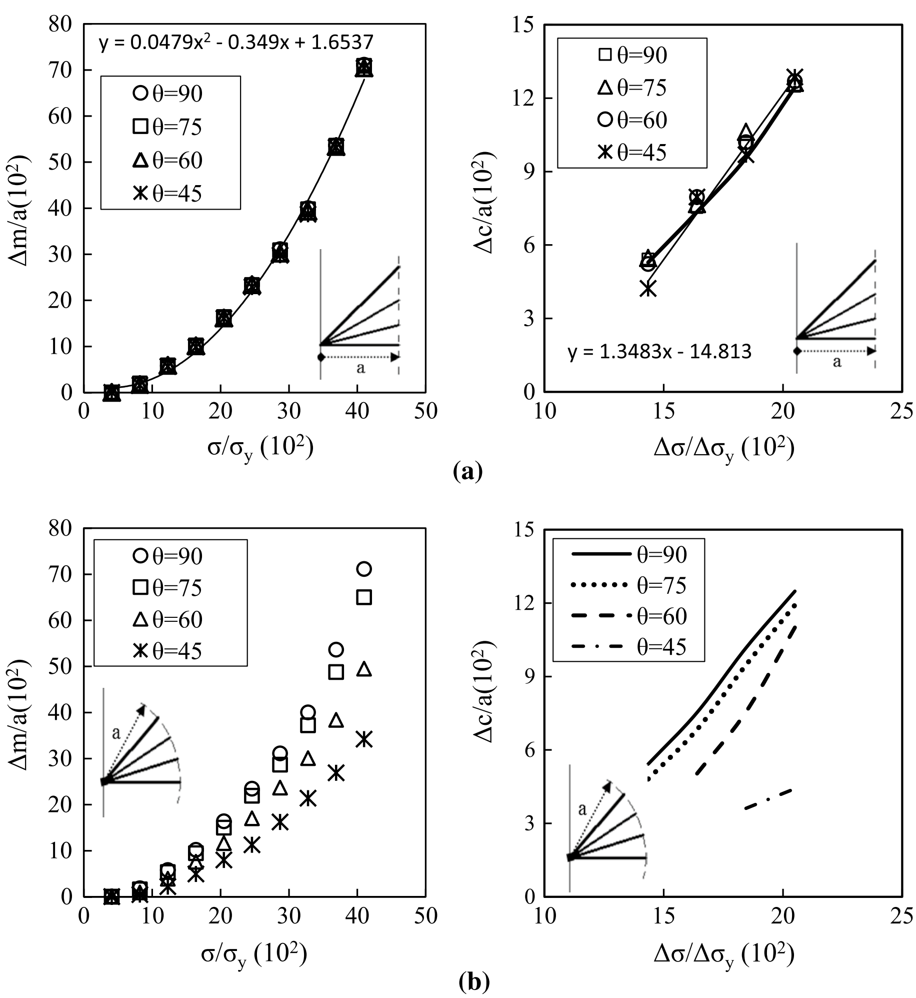

Fig. 15 Monotonic and cyclic plastic zone sizes for the two cases: **a** ECHP and **b** ECIL

angles. The proportionality constant can be evaluated by fitting a linear equation to the Δc data. From these results, the relation between (Δc/a) and ($\Delta\sigma/\Delta\sigma_{y}$), independent of the crack inclination angle, can be expressed as:

$$\Delta c = a\left[0.674\left(\frac{\Delta\sigma_i}{\sigma_y}\right) - 0.148\right] \quad \text{for } a/w = 0.3 \tag{7}$$

4.4 Δm and ΔC for EICL

The variation of monotonic and cyclic plastic zone size, Δm and Δc versus the applied stress σ for different crack angles θ is shown in Fig. 15b. This figure indicates that the magnitude of Δm and Δc increased as the inclination angle θ increased. It is interesting to note that the cyclic plastic zone Δc is delayed to appear with decreasing the inclination angle θ. For example, for θ = 90° the cyclic plastic zone appeared at Δσ = 103.32 MPa, while for θ = 45° the cyclic plastic zone appeared at Δσ = 132.84 MPa.

4.5 Monotonic CTOD and Cyclic ΔCTOD

Experimental studies showed that crack closure behavior cannot fully describe the measured FCG under mixed mode I/II loading (Biner 2001). CTOD of an inclined crack under static loading can be used as a fracture parameter to predict the crack initiation angle (Ma et al. 1999). Crack tip opening displacement (CTOD) and crack tip sliding displacement (CTSD) are investigated further in the next sections.

4.6 CTOD and ΔCTOD for ECHP

The variations of CTOD and CTSD behind the crack tip of an inclined crack with the applied stress σ are illustrated in Fig. 16. For the same σ/σ_y, the normalized CTOD increased with increasing the crack inclination angle θ (For ECHP). However, the CTSD show opposite trend. This may be indicated that, the resultant of the CTOD components independent of the crack inclination angle θ for ECHP. It worth to note that, such cracks have a different actual crack lengths with constant horizontal projection, hence, these cracks take into consideration the effect of crack inclination angle through their lengths. The resultant of the CTOD, which is normal to the crack faces, and the CTSD, which is tangent to the crack faces, is calculated from Eq. (8), and is plotted in Fig. 16.

$$CTOD_R = \sqrt{CTOD^2 + CTSD^2} \tag{8}$$

For the normalized $CTOD_R$, it's observed from Fig. 17 that for any angle, the increase of $CTOD_R$ is proportional to the applied stress. The proportionality constant can be evaluated by fitting a polynomial equation to all the $CTOD_R$ data. From these results, the relation between ($CTOD_R$) and (σ),

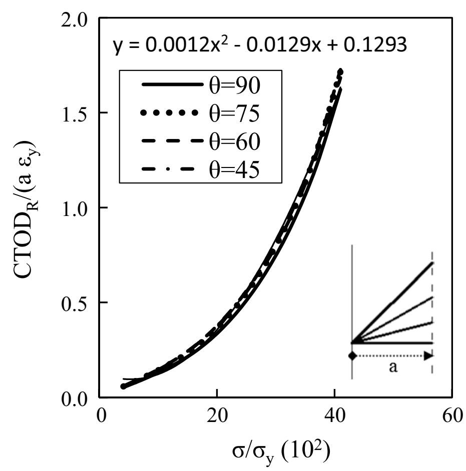

Fig. 17 Variation of the resultant $CTOD_R$ near the tip of the present inclined crack

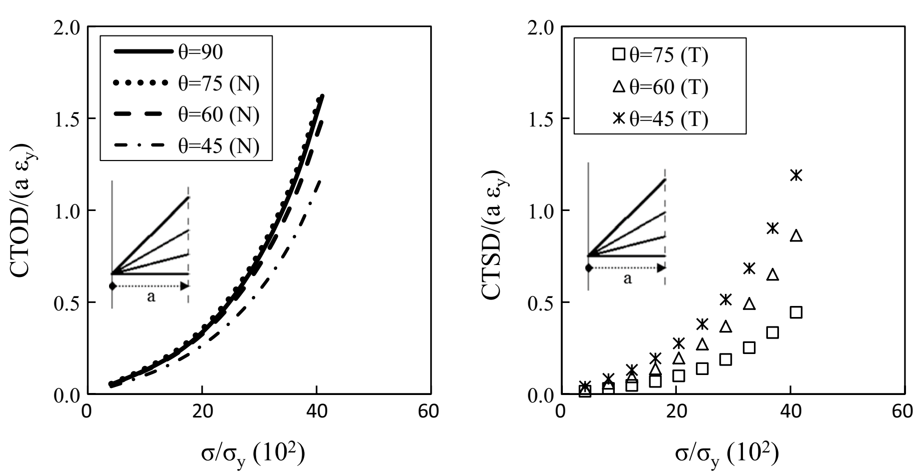

Fig. 16 Variation of computed CTOD and CTSD behind the tip of the present inclined crack with different inclination angles θ for the ECHP case

independent of the crack inclination angle, can be expressed as:

$$CTOD_R = a\left[12\left(\frac{\sigma_i^2}{\sigma_y E}\right) - 1.29\left(\frac{\sigma_i}{E}\right) + 0.129\left(\frac{\sigma_y}{E}\right)\right] \quad \text{for } a/w = 0.3 \tag{9}$$

And then the CTOD and CTSD can be calculated by the analysis of the resultant $CTOD_R$, and are given in Eqs. (10) and (11).

$$CTOD = \left(a\left[12\left(\frac{\sigma_i^2}{\sigma_y E}\right) - 1.29\left(\frac{\sigma_i}{E}\right) + 0.129\left(\frac{\sigma_y}{E}\right)\right]\right)\cos\theta \tag{10}$$

$$CTSD = \left(a\left[12\left(\frac{\sigma_i^2}{\sigma_y E}\right) - 1.29\left(\frac{\sigma_i}{E}\right) + 0.129\left(\frac{\sigma_y}{E}\right)\right]\right)\sin\theta \tag{11}$$

Figure 18 shows that the normalized cyclic ΔCTOD increased with increasing the crack inclination angle θ, while the ΔCTSD increased with decreasing the crack inclination angle θ. The resultant of ΔCTOD, which is normal to the crack faces, and the ΔCTSD, which is tangent to the crack faces, is calculated as shown in Fig. 19. For the normalized $\Delta CTOD_R$, it's observed that for any angle, the increase of $\Delta CTOD_R$ is proportional to the applied stress (σ). The proportionality constant can be evaluated by fitting a polynomial equation to all the $\Delta CTOD_R$ data. From these results, the relation between ($\Delta CTOD_R$) and (Δσ), independent of the crack inclination angle, can be expressed as:

$$\Delta CTOD_R = a\left[10^2\left(\frac{\Delta\sigma_i^2}{2\sigma_y E}\right) - 0.9\left(\frac{\Delta\sigma_i}{E}\right) + 0.012\left(\frac{\sigma_y}{E}\right)\right] \tag{12}$$

And then the ΔCTOD and ΔCTSD can be calculated by the analysis of the resultant $\Delta CTOD_R$, and are given in Eqs. (13) and (14).

$$\Delta CTOD = \left(a\left[10^2\left(\frac{\Delta\sigma_i^2}{2\sigma_y E}\right) - 0.9\left(\frac{\Delta\sigma_i}{E}\right) + 0.012\left(\frac{\sigma_y}{E}\right)\right]\right)\cos\theta \tag{13}$$

$$\Delta CTSD = \left(a\left[10^2\left(\frac{\Delta\sigma_i^2}{2\sigma_y E}\right) - 0.9\left(\frac{\Delta\sigma_i}{E}\right) + 0.012\left(\frac{\sigma_y}{E}\right)\right]\right)\sin\theta \tag{14}$$

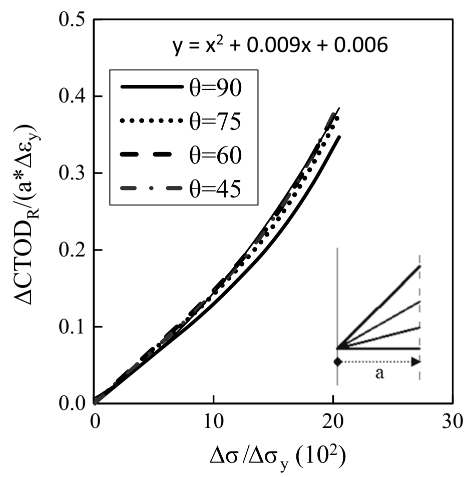

Fig. 19 Variation of the resultant $\Delta CTOD_R$ near the tip of the inclined crack

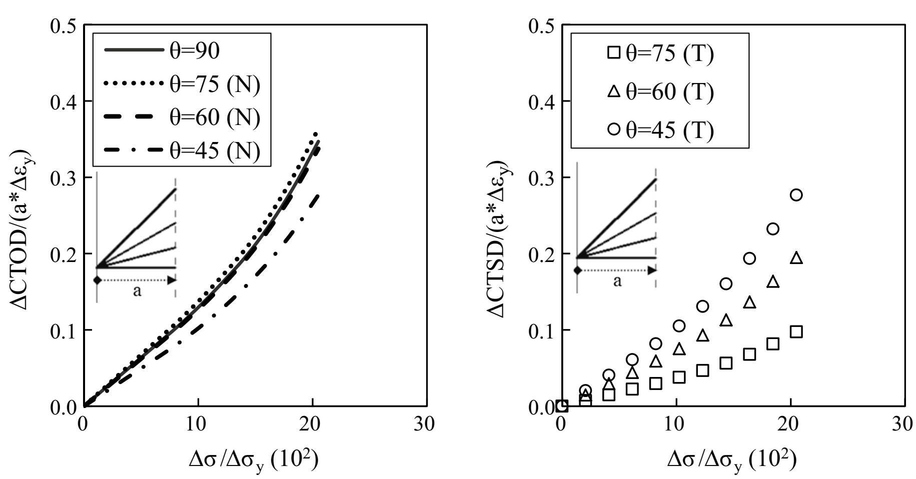

Fig. 18 Variation of computed ΔCTOD and ΔCTSD behind the tip of the inclined crack with different inclination angles θ for the ECHP case

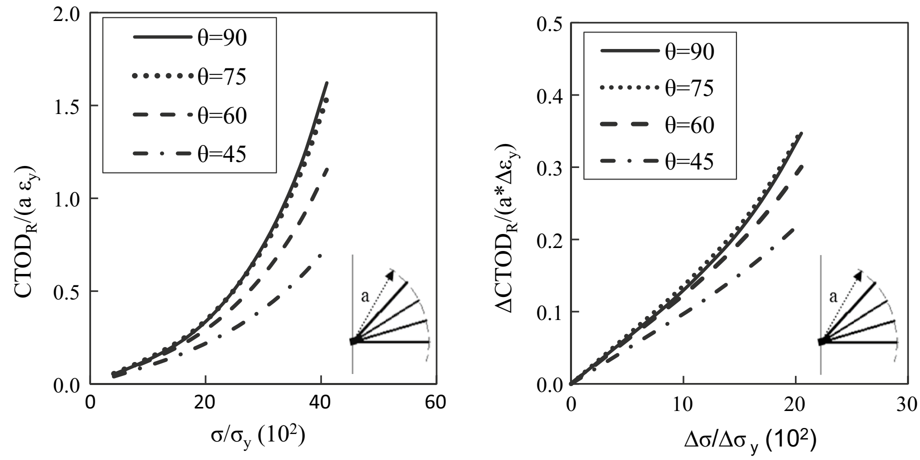

Fig. 20 Variation of the resultant $\Delta CTOD_R$ and $\Delta CTSD_R$ near the tip of the inclined crack for the EICL case

4.7 $CTOD_R$ and $\Delta CTOD_R$ for EICL

The variation of the resultant CTODR and ΔCTODR of the inclined crack with the applied stress, σ for the EICL cases is illustrated in Fig. 20. The normalized monotonic CTODR increased with increasing the crack inclination angle θ. The same results were also obtained for the ΔCTODR. It was also observed that the results for a crack with θ = 90 degrees are close to the results for the crack with θ = 75 degrees than the results for θ = 45, and 60.

5 Conclusions

The characteristics of monotonic and cyclic crack tip deformation were analyzed for different crack inclination angels and stress levels. The following conclusions were determined based on the results of the study presented in this paper:

1. The finite element results were compared well to the analytical results based on Dugdale's model.
2. In the equal crack horizontal projection (ECHP) case, the variation of monotonic and cyclic crack tip plastic zone size appears to be almost the same for different crack inclination angles.
3. For the equal inclined crack length (EICL) case, the commencement of Δc appears at high stress range with decreasing the inclination angle θ. For example, for θ = 90° the cyclic plastic zone appeared at Δσ = 103.32 MPa, while for θ = 45° the cyclic plastic zone appeared at Δσ = 132.84 MPa.
4. In the case of ECHP, the monotonic and cyclic CTOD are directly proportional to θ, while, the monotonic and cyclic CTSD are inversely proportional to θ.
5. The monotonic resultant crack tip opening displacement ($CTOD_R$) and the cyclic resultant ($\Delta CTOD_R$) are independent of the crack inclination angle for the ECHP case.

References

ANSYS release 14.5 documentation. ANSYS Inc.

Biner, S. B. (2001). Fatigue crack growth studies under mixed-mode loading. *International Journal of Fatigue, 23,* S259–S263.

Chang, T., & Guo, W. (1999). Effects of strain hardening and stress state on fatigue crack closure. *International Journal of Fatigue, 21,* 881–888.

Dugdale, D. S. (1963). Yielding of steel containing slits. *Journal of the Mechanics and Physics of Solids, 8,* 103.

Elber, W. (1970). Fatigue crack closure under cyclic tension. *Engineering Fracture Mechanics, 2,* 37–45.

Elber, W. (1971). The significance of fatigue crack closure. In *Damage tolerance in aircraft structures* (pp. 230–242). ASTM STP486. https://ntrs.nasa.gov/search.jsp?R=19710054465.

El-Emam, H., Salim, H., & Sallam, H. (2016). Composite patch configuration and prestraining effect on crack tip deformation and plastic zone for inclined cracks. *Journal of Composites for Construction, 20*(4), 04016002. https://doi.org/10.1061/(ASCE)CC.1943-5614.0000655,04016002.

El-Emam, H., Salim, H., & Sallam, H. (2017). Composite patch configuration and prestress effect on SIFs for inclined cracks in steel plates. *Journal of Structural Engineering, 143*(5), 04016229. https://doi.org/10.1061/(ASCE)ST.1943-541X.0001727.

Hammouda, M. M. I., Ahmad, S. E., & Sallam, H. E. M. (1995). Correlation of fatigue crack growth by crack tip deformation behavior. *Fatigue and Fracture of Engineering Materials and Structures, 18*(1), 93–104.

Hammouda, M. M. I., Ahmad, S. E., Sherbini, A. S., & Sallam, H. E. M. (1999). Deformation behaviour at the tip of physically short fatigue crack due to a single overload. *Fatigue and Fracture of Engineering Materials and Structures, 22*(2), 145–151.

Hammouda, M. M. I., Fayed, A. S., & Sallam, H. E. M. (2002). Mode II stresses intensity factors for central slant cracks with frictional surfaces in uniaxially compressed plates. *International Journal of Fatigue, 24*(12), 1213–1222.

Hammouda, M. M. I., Fayed, A. S., & Sallam, H. E. M. (2003a). Simulation of mixed mode I/II cyclic deformation at the tip of a short kinked inclined crack with frictional surfaces. *International Journal of Fatigue, 25,* 743–753.

Hammouda, M. M. I., Fayed, A. S., & Sallam, H. E. M. (2003b). Stress intensity factors of a shortly kinked slant central crack with frictional surfaces in uniaxially loaded plates. *International Journal of Fatigue, 25*(4), 283–298.

Hammouda, M. M. I., Osman, H. G., & Sallam, H. E. M. (2004a). Mode I notch fatigue crack growth behaviour under constant amplitude loading and due to the application of a single tensile overload. *International Journal of Fatigue, 26*(2), 183–192.

Hammouda, M. M. I., Sallam, H. E. M., & Osman, H. G. (2004b). Significance of crack tip plasticity to early notch fatigue crack growth. *International Journal of Fatigue, 26*(2), 173–182.

Hannachi, M. T., & Djebaili, H. (2013). Analysis of the elastic energy and crack tip opening displacement with increased yield stress. *Journal of Science and Engineering, 2,* 163–172.

Isida, N. (1966). Stress-intensity factors for the tension of an eccentrically cracked strip. *Journal of Applied Mechanics, 33*(3), 674–675.

Ma, F., Deng, X., Sutton, M.A., & Newman, Jr. (1999). *A CTOD-based mixed-mode fracture criterion. ASTM STP9* (vol. 135, pp. 86–110).

McEvily, A. J. (2009). On the cyclic crack-tip opening displacement. *Fatigue and Fracture of Engineering Materials and Structures, 32,* 284–285.

Murakami, Y. (1987). *Stress intensity factor handbook* (Vol. 1). Oxford: Pergamon Press.

Para, A. F., Sanjust, V., Shoptaw, S., Jarvik, M. E., Ling, W., Rawson, R. A., et al. (1996). Plastic zone size in fatigue cracking. *International Journal of Pressure Vessels and Piping, 68,* 279–285.

Paul, S. K., & Tarafder, S. (2013). Cyclic plastic deformation response at fatigue crack tips. *International Journal of Pressure Vessels and Piping, 101,* 81–90.

Plank, R., & Kuhn, G. (1999). Fatigue crack propagation under non-proportional mixed mode loading. *Engineering Fracture Mechanics, 62,* 203–229.

Qian, J., & Fatemi, A. (1996). Fatigue crack growth under mixed-mode I and II loading. *Fracture of Engineering Materials & Structures, 19,* 1277–1284.

Qian, J., & Fatemi, A. (1999). Fatigue cracking behavior of 1045 HR steel subjected to mixed-mode I and II loading, Part II: Crack growth behavior and predictions. In T. Cordes & K. Lease (Eds.), *Multi-axial fatigue of an induction hardened shaft* (pp. 165–174). Warrendale, PA: Society of Automotive Engineers.

Reddy, S. C., & Fatemi, A. (1992). *Small crack growth in multiaxial fatigue* (vol. 112, pp. 276–298). ASTM STP2. https://doi.org/10.1520/STP24164S.

Rice, J. R. (1967). Mechanics of crack tip deformation and extension by fatigue. In *Fatigue crack propagation* (pp. 247–310). ASTM STP 415. https://doi.org/10.1520/STP47234S.

Soh, A. K., & Bain, L. C. (2001). Mixed mode fatigue crack growth criteria. *International Journal of Fatigue, 23,* 427–439.

Suresh, S. (1998). *Fatigue of materials* (2nd ed.). Cambridge: Cambridge University Press.

Tada, H., Paris, P. C., & Irwin, G. R. (1973). *The stress analysis of cracks handbook*. Hellertown, PA: Del Research Corp.

Wells, A. A. (1963). Application of fracture mechanics at and beyond general yielding. *British Welding Journal, 10–11,* 563–570.

Wong, S. L., Bold, P. E., Brown, M. W., & Allen, R. J. (2000). Fatigue crack growth rates under sequential mixed-mode I and II loading cycles. *Fatigue and Fracture of Engineering Materials and Structures, 23,* 667–674.

You, B. R., & Lee, S. B. (1998). Fatigue crack growth behavior of SM45Csteel under mixed-mode I and II loading. *Fatigue and Fracture of Engineering Materials and Structures, 21,* 1037–1048.

Zhang, W., & Liu, Y. (2011). Plastic zone size estimation under cyclic loadings using in situ optical microscopy fatigue testing. *Fatigue and Fracture of Engineering Materials and Structures, 34,* 717–727.